Isotropic exchange interaction between Mo and the proximal FeS center in the xanthine oxidase family member aldehyde oxidoreductase from Desulfovibrio gigas *on native and polyalcohol inhibited samples: an EPR and QM/MM study*

María C. Gómez, Nicolás I. Neuman, Sergio D. Dalosto, Pablo J. González, et al.

JBIC Journal of Biological Inorganic Chemistry

ISSN 0949-8257
Volume 20
Number 2

J Biol Inorg Chem (2015) 20:233-242
DOI 10.1007/s00775-014-1204-8

Springer

J Biol Inorg Chem (2015) 20:233–242
DOI 10.1007/s00775-014-1204-8

ORIGINAL PAPER

Isotropic exchange interaction between Mo and the proximal FeS center in the xanthine oxidase family member aldehyde oxidoreductase from *Desulfovibrio gigas* on native and polyalcohol inhibited samples: an EPR and QM/MM study

María C. Gómez · Nicolás I. Neuman · Sergio D. Dalosto · Pablo J. González · José J. G. Moura · Alberto C. Rizzi · Carlos D. Brondino

Received: 9 July 2014 / Accepted: 7 October 2014 / Published online: 25 October 2014

Abstract Aldehyde oxidoreductase from *Desulfovibrio gigas* (*Dg*AOR) is a homodimeric molybdenum-containing protein that catalyzes the hydroxylation of aldehydes to carboxylic acids and contains a Mo-pyranopterin active site and two FeS centers called FeS 1 and FeS 2. The electron transfer reaction inside *Dg*AOR is proposed to be performed through a chemical pathway linking Mo and the two FeS clusters involving the pyranopterin ligand. EPR studies performed on reduced as-prepared *Dg*AOR showed that this pathway is able to transmit very weak exchange interactions between Mo(V) and reduced FeS 1. Similar EPR studies but performed on *Dg*AOR samples inhibited with glycerol and ethylene glycol showed that the value of the exchange coupling constant J increases ~ 2 times upon alcohol inhibition. Structural studies in these *Dg*AOR samples have demonstrated that the Mo–FeS 1 bridging pathway does not show significant differences, confirming that the changes in J observed upon inhibition cannot be ascribed to structural changes associated neither with pyranopterin and FeS 1 nor with changes in the electronic structure of FeS 1, as its EPR properties remain unchanged. Theoretical calculations indicate that the changes in J detected by EPR are related to changes in the electronic structure of Mo(V) determined by the replacement of the OHx labile ligand for an alcohol molecule. Since the relationship between electron transfer rate and isotropic exchange interaction, the present results suggest that the intraenzyme electron transfer process mediated by the pyranopterin moiety is governed by a Mo ligand-based regulatory mechanism.

Keywords Aldehyde oxidoreductase · Molybdenum · Exchange interaction · EPR · QM/MM

Abbreviations

*Dg*AOR Aldehyde oxidoreductase from *Desulfovibrio gigas*

Responsible Editors: José Moura and Paul Bernhardt.

M. C. Gómez · N. I. Neuman · P. J. González · A. C. Rizzi · C. D. Brondino (✉)
Departamento de Física, Facultad de Bioquímica y Ciencias Biológicas, Universidad Nacional del Litoral, Ciudad Universitaria, Paraje El Pozo, S3000ZAA Santa Fe, Argentina
e-mail: brondino@fbcb.unl.edu.ar

S. D. Dalosto
Instituto de Física del Litoral, CONICET-UNL, Güemes 3450, S3000ZAA Santa Fe, Argentina

J. J. G. Moura
REQUIMTE/CQFB, Departamento de Quimica, Faculdade de Ciências e Tecnologia, Universidade Nova de Lisboa, 2829-516 Caparica, Portugal

Introduction

The study of spin systems coupled with isotropic exchange interaction ($H_{ex} = -J\ S_1 \cdot S_2$), also known as superexchange interaction when a bridging ligand is involved, is a research field that constitutes a cross point between biology and physical chemistry [1–10]. The sign and magnitude of the isotropic exchange parameter J is related to the nature and structural topology of the bridging chemical path and the properties of the magnetic orbitals of the interacting spins. Important efforts have been devoted to establish magneto structural correlations in the last decades [11], information which is advantageously used today to design

materials with predictable magnetic properties [12–14]. Such correlations are also of interest in biology, as several redox proteins contain exchange coupled paramagnetic centers in their structures [1, 5–7, 9, 10, 15–18]. For biological systems, the evaluation of J is not only relevant to understand the electronic properties of the redox centers, but also to learn on structural and functional aspects of the systems that complement information obtained from conventional structural and kinetic techniques [18–20]. Particularly, the analysis of the magnetic interaction between centers can be advantageously used to determine inter-center distances, to assign the EPR active centers with those of the structure, and to study the integrity of the electron transfer pathways in distinct protein conditions [21–26]. Additional interest in the evaluation of exchange interactions is that the rate of electron transfer through a chemical path linking two paramagnetic centers is proportional to $|J|$ under conditions of maximal rate, which means that the value of $|J|$ can be advantageously used to predict the ability of the chemical path as electron transfer conduit [23].

The redox cofactors in mononuclear molybdenum-containing enzymes of the xanthine oxidase (XO) family are examples of weakly exchange coupled centers in biological systems [19, 20, 27]. These enzymes catalyze the oxidative hydroxylation of aldehydes and N-heterocycles by transferring an oxygen atom from water to the substrate in reactions that imply a net exchange of two electrons between enzyme and substrate [28]. The accepted reaction mechanism implies the reaction of substrate with the molybdenum center, which is reduced from Mo(VI) to Mo(IV). The two involved reducing equivalents are transferred to an external electron acceptor (NAD^+ or dioxygen) by means of an electron transfer chain which may include, besides the Mo cofactor, metal and nonmetal redox centers (usually situated $\sim$10–20 Å away) linked by different types of bridging chemical paths. All these centers may be paramagnetic in some oxidation states, and despite both the long distances and chemical paths, they can present weak magnetic couplings produced by electron spin–spin interactions such as the above-mentioned isotropic exchange [19, 20, 27].

Aldehyde oxidoreductase from *Desulfovibrio gigas* (*Dg*AOR) is a homodimeric mononuclear Mo-containing protein ($\sim$100 kDa per monomer) that belongs to the XO family, but does not contain an equatorial sulfido ligand at the Mo site [29–31]. Each of the monomers, which are catalytically independent [32], is organized into two major domains called Mo and FeS domains. The Mo domain is the largest one and contains the active site, whereas the FeS domain contains two [2Fe–2S] centers called FeS 1 and FeS 2. The electron transfer reaction inside *Dg*AOR is proposed to be performed through a chemical pathway linking the Mo atom and the two FeS clusters, a motif that is common to most XO family members, which may present some differences at the Mo site and longer electron transfer chains [33, 34]. The proposed electron transfer pathway between Mo center and FeS 1 in *Dg*AOR is shown in Fig. 1. This pathway is formed by the pyranopterin ligand and a sulfur atom from Cys 139, where the N from the pyranopterin is hydrogen bonded to the Cys 139 sulfur. Electron paramagnetic resonance (EPR) studies performed on as-prepared *Dg*AOR reduced with sodium dithionite showed that this pathway is able to transmit very weak exchange interactions [17, 21, 22, 27]. Similar studies but performed on *Dg*AOR samples treated with inhibitors such as glycerol (GOL) and ethylene glycol (EDO) showed that the J value depends on the nature of the inhibitor [31]. However, a detailed comparison of the structure of as-purified *Dg*AOR with those reacted with GOL and EDO showed no significant changes in the nature and structural topology of the chemical path between Mo and FeS 1, which is in apparent contradiction with the fact that J depends on the structural characteristic of the chemical

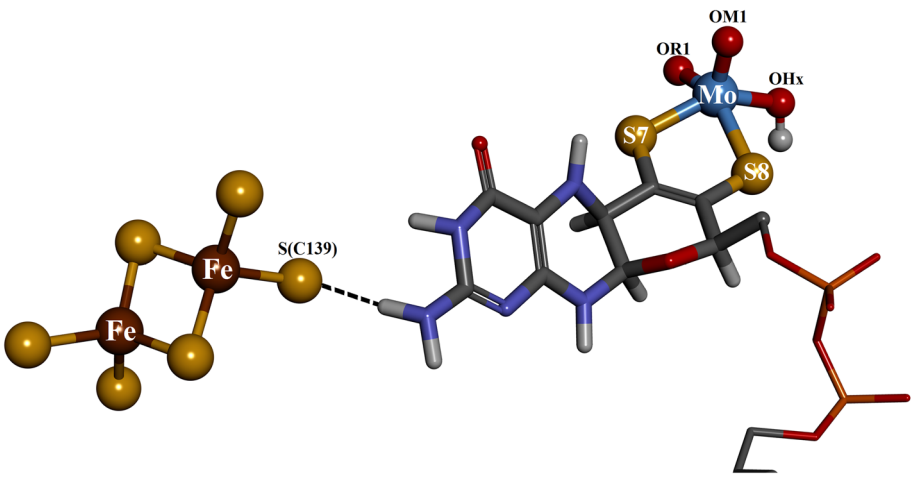

Fig. 1 The Mo-pyranopterin cytidine dinucleotide cofactor and the proximal [2Fe–2S] cluster present in *Dg*AOR. The pyranopterin portion of the Mo cofactor is the proposed electron transfer pathway between the Mo atom and the FeS 1 center in *Dg*AOR. The pyranopterin moiety with its hydrogen bond interaction with the C139 S atom is displayed. The *labels* on the metal ligands are according to the crystallography for native *Dg*AOR [30]

path. The elucidation of the factors responsible for these changes in J is important to understand the role of the electronic structure of the Mo(V) site in facilitating the Mo–FeS 1 electron transfer, which constitutes the object of this paper.

In this paper, we investigate by EPR and computational methods using first principles combined with molecular mechanics (QM/MM) the factors that govern the Mo–FeS 1 exchange interaction in as-prepared *Dg*AOR reduced with dithionite and in reduced *Dg*AOR reacted with glycerol and ethylene glycol. We analyze how the changes at the Mo site upon alcohol inhibition affect its electronic structure and hence the transmission of the isotropic exchange interaction between Mo and FeS1. The implications of these results in the intraenzyme electron transfer process are also discussed.

Materials and methods

Sample preparation

*Dg*AOR was purified as reported previously [35, 36]. EDO- and GOL-reacted samples for EPR spectroscopy were prepared according to the procedures published elsewhere [31].

EPR spectroscopy

X-band CW-EPR spectra of *Dg*AOR were obtained on a Bruker EMX-Plus spectrometer, equipped with an Oxford Instrument helium continuous-flow cryostat and a rectangular cavity with 100 kHz field modulation. EPR spectra were simulated with the EasySpin toolbox based on MATLAB® [37]. The g-values for Mo were taken from the high-temperature spectra assuming only a Zeeman term, and those for FeS1 from spectra at 50 K where no magnetic coupling FeS1–FeS2 was detected. These g-values were used to simulate the split Mo(V) signal resulting from the magnetic coupling Mo(V)–FeS1. More details are given under the section "Analysis of the Mo(V)–FeS 1 magnetic coupling".

Computational methods

Quantum mechanics and molecular mechanics (QM/MM) calculations were performed to study the interaction of *Dg*AOR with the inhibitors GOL and EDO. The software package used was Gaussian 09 [38].

Spin-polarized WB97XD functional including empirical dispersion [39] and an Amber classical force field was used for the QM and MM studies, respectively. The basis set for the Mo atom was Lanl2DZ [40, 41], which includes relativistic correction, and 6-31G* for the rest of the atoms in the QM part. This basis set was used to evaluate the catalytic mechanisms of XO and AOR [42, 43]. To focus on the pyranopterin moiety and on the Mo site, we have removed the cytidine dinucleotide group and replaced the terminal methylene group by a methyl group, which is called Mo-cof hereafter. The Mo-cof, the inhibitor, and the Glu869 residue were treated with QM, whereas the rest of the protein with MM. The buried water molecules in the active site were conserved and MM-treated. To obtain the most favorable structure, the Mo-cof, the inhibitor, and the COO^- group of Glu869 (all of them in the QM part) were allowed to fully relax, meanwhile only the H atoms of the MM part were allowed to relax. Since we are primarily interested in the EPR-detected species, we computed Mo-cof(V) with and without the inhibitor and with the Mo oxygen ligands as oxo or hydroxo, depending on the case. As the crystallographic structures were reported for the *Dg*AOR Mo-cof(VI) forms with and without the inhibitor, we computed the relaxed structure for these cases and compared them with the Mo-cof(V). The initial structure of *Dg*AOR used along the computations was based on the 1VLB accession code, which we call native and has the Mo atom in +VI oxidation state [30]. The inhibitor was added to the native structure at the Mo-cof site according with the positions reported in the 3FAH and 3FC4 accession codes for GOL and EDO, respectively [31]. This does not impose any bias since the position of the inhibitor was fully relaxed. Although the crystallographic structures for native *Dg*AOR show that two of the Mo oxygen ligands named OM1 (apical) and OR1 (equatorial) are oxo ligands and the other equatorial ligand is an hydroxo (OHx, see Fig. 1), we have computed different protonation states for these oxygen atoms, i.e., Mo(OM1-OR1-OH), Mo(OM1-O(H)R1-OH), Mo(OM1-OR1-O) without the inhibitor and Mo(OM1-O(H)R1), Mo(O(H)M1-OR1) and Mo(OM1-OR1) for the inhibited enzyme to look for the most energetically stable structure. Computation of these variants is necessary as the crystal structures were obtained for the enzyme in the Mo(VI) state and we are interested primarily in the EPR-active Mo(V) state. Besides, for the EDO- and GOL-reacted *Dg*AOR, the O_2 atom of both inhibitors was considered to be protonated. One of the reasons for our assumption was the high pKa of the alcohol moiety in aqueous medium ($\sim$14), which suggests that these polyalcohols are fully protonated in the bulk solution before entering into the substrate channel, and the other is the reversible character of both alcohols as inhibitors and the value of the competitive inhibition constants (K_{iC}), which suggest that the alcohol molecule does not bind to the Mo ion stronger than the substrate [31] and the irreversible inhibitor arsenite [44]. However, since the interaction Mo–O_2 could lower the alcohol pKa, we evaluated the energetic

of alcohol–*Dg*AOR interaction but with alkoxide forms. The results indicate that the alcohol protonated forms are energetically more favorable than the non-protonated ones. Hence, the results reported correspond to the protonated forms of both alcohols.

Results and discussion

EPR spectroscopy

Figure 2, spectra a, b, shows the EPR signals at 140 K obtained from active samples of as-purified and D_2O-exchanged *Dg*AOR upon reduction with excess dithionite for 20 min under anaerobic conditions. The Mo(V) signal obtained under these conditions is commonly named slow signal in the literature on Mo enzymes [28], and is detected over the temperature range 4–150 K. The slow signal shows nearly axial symmetry ($g_1 = 1.971$, $g_2 = 1.969$, $g_3 = 1.959$) and hyperfine structure with a species with $I = ½$ ($A_1 = A_2 = 13.8 \times 10^{-4}$ cm^{-1}, $A_3 = 14.6 \times 10^{-4}$ cm^{-1}) (Fig. 2, spectrum a). The nuclear species with $I = 1/2$ corresponds to a solvent exchangeable proton as demonstrated from the spectrum of *Dg*AOR in a D_2O-exchanged sample (Fig. 2, spectrum b). Figure 2, spectra c, d, shows the EPR signals of the same samples under the same experimental conditions but at 20 K, which in addition show the EPR signals corresponding to the two FeS centers (FeS 1, $g_1 = 2.023$, $g_2 = 1.938$, $g_3 = 1.919$; FeS 2, $g_1 = 2.060$, $g_2 = 1.998$, $g_3 = 1.900$). Whereas ~100 % of the FeS centers are paramagnetic under these conditions, only about 10 % of the total molybdenum is obtained as Mo(V) species. The splitting of the Mo(V) signal at 20 K is due to magnetic coupling with FeS 1. This splitting is not observed at higher temperatures because of the high relaxation rate of FeS 1, a phenomenon which was analyzed previously [17]. The FeS 1 signal splitting produced by coupling with the Mo(V) center should also be observed, but as only about 10 % of the Mo–FeS 1 pair is magnetically coupled, it cannot be detected. The splitting at g_1 of FeS 1 signal is due to the magnetic coupling with FeS 2, which will be not analyzed here. The EPR spectra of dithionite-reduced *Dg*AOR samples reacted with EDO (Fig. 2, spectra e, g) or GOL (Fig. 2, spectra f, h) show also EPR signals associated with the different metal cofactors of the enzyme. EPR spectra e and f at 140 K are associated with Mo(V) species, whereas the spectra at 20 K (spectra g and h) show in addition to the Mo(V) signal, the signals associated with the two FeS clusters.

The spectra associated with the FeS centers in all *Dg*AOR forms shown in Fig. 2 have *g*-values and temperature dependence (not shown) essentially identical. This

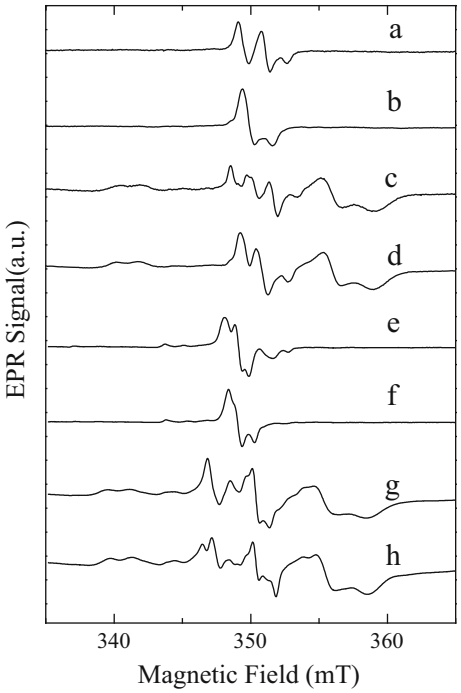

Fig. 2 EPR spectra of dithionite-reduced *Dg*AOR under different experimental conditions at two temperatures. *a*, *b* Slow signal in normal water and D_2O, respectively, at 140 K. *c*, *d* Idem *a* and *b*, respectively, but at 20 K. *e*, *f* EDO- and GOL-inhibited *Dg*AOR, respectively, at 140 K. *g*, *h* Idem *e* and *f*, respectively, but at 20 K. The microwave frequency was 9.65 GHz. Minor features observed specially in the signals on the inhibited samples correspond to the hyperfine structure given by the nuclear spin of the ^{95}Mo and ^{97}Mo isotopes ($I = 5/2$, natural abundancy: 15.90 and 9.60 %, respectively) and also to a small component of slow-type EPR signal likely arising from uninhibited enzyme molecules [31]

suggests that neither the structure nor the chemical paths connecting FeS centers are affected on inhibition, which was also confirmed by X-ray crystallography [20]. However, the Mo(V) EPR signals do present significant differences upon *Dg*AOR inhibition. The Mo(V) signals observed in EDO- and GOL-inhibited *Dg*AOR at 140 K (spectra e and f) show rhombic symmetry (EDO, $g_1 = 1.978$, $g_2 = 1.972$, $g_3 = 1.968$; GOL, $g_1 = 1.977$, $g_2 = 1.973$, $g_3 = 1.966$) [31], in contrast to the axial spectrum obtained in dithionite-reduced as-prepared *Dg*AOR. The spectra obtained in D_2O-exchanged samples of *Dg*AOR reacted with normal and ^{2}H-enriched alcohols (not shown) are very similar to those obtained in normal water, in line with results reported for ethylene glycol-reacted desulfo-bovine milk XO [45]. The Mo(V) signals at 20 K shown in Fig. 2, spectra g, h, are also split by magnetic coupling with FeS 1. As observed, the Mo(V) signal splitting of the alcohol-inhibited *Dg*AOR is ~2 times larger than that observed for the slow signal, suggesting that the Mo–FeS 1 exchange interaction increased significantly upon alcohol inhibition.

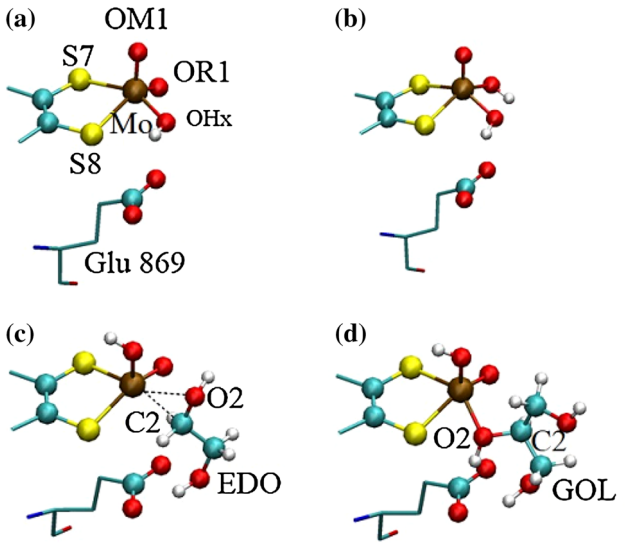

Fig. 3 Proposed structures for the Mo(V) EPR active centers. **a** As-prepared Mo(VI) form, as determined by X-ray crystallography, see text. **b** Mo(V) center associated with the slow EPR signal. **c**, **d** EDO- and GOL-inhibited *Dg*AOR, respectively

Figure 3 shows the proposed structures of the Mo centers associated with the EPR signals shown in Fig. 2. The structure for the as-prepared Mo(VI) form is shown in Fig. 3a for comparison [29, 30]. Figure 3b shows the structure proposed for the Mo(V) species associated with the slow EPR signal. This structure is proposed on the basis of EPR and ENDOR studies in desulfo inhibited XO [46, 47] and EPR studies on arsenite-reacted *Dg*AOR [26], which suggested that the equatorial oxo ligand is susceptible to protonation.

Structures c and d, which were obtained by X-ray techniques [31], may not necessarily be associated with the EPR signals shown in Fig. 2e–h, as Mo was proposed to be as Mo(VI). However, note that the interaction between alcohols and the Mo(VI) ion distorts the nearly square pyramidal coordination, which is in line with the rhombic Mo(V) EPR signal of alcohol-reacted enzymes. As EDO- and GOL-reacted D_2O-exchanged *Dg*AOR showed the same type of EPR signals (no solvent exchangeable proton was observed) [31], we will use these structures for the Mo(V) centers in the alcohol-inhibited enzyme as starting point in the computational calculations presented below.

Analysis of the Mo(V)–FeS 1 magnetic coupling

*Dg*AOR is a three-spin system and therefore should be analyzed with a full spin Hamiltonian including the Zeeman terms associated with the three-spin centers and the exchange interactions between them. However, as explained above and elsewhere [21, 22], the splitting experienced by Mo(V) is solely due to the interaction Mo(V)–FeS1, whereas the splitting of the FeS1 EPR signal at g_{max} is provoked by magnetic coupling with FeS2. So the spectra shown in Fig. 2 can be interpreted assuming two independent pairs of interacting spin ½ centers. Note that the exchange interaction Mo(V)–FeS2 should be transmitted by a very long chemical path (distance Mo–FeS2 ~24 Å) and to the best of our knowledge, no exchange interaction has been detected for such long chemical path, which gives an additional support to our assumption. As this paper deals with the exchange interaction mediated by the pyranopterin ligand, we considered in our analysis only the pair Mo(V)–FeS1.

The spin Hamiltonian for a pair of interacting $S = 1/2$ centers can be written as:

$$\mathbf{H} = \mu_B\left(\vec{\mathbf{S}}_1 \cdot \mathbf{g}_1 + \vec{\mathbf{S}}_2 \cdot \mathbf{g}_2\right) \cdot \vec{\mathbf{B}} + \vec{\mathbf{S}}_1 \cdot (-J\,\mathbf{I} + \mathbf{D}) \cdot \vec{\mathbf{S}}_2 \quad (1)$$

where $\mathbf{g}_1$ and $\mathbf{g}_2$ are the **g**-tensors associated with the interacting Mo(V) and FeS 1 centers, respectively, J is the isotropic exchange interaction constant, **I** is the unit matrix, **D** is a second rank symmetric tensor with a trace of zero, and all the other symbols have their usual meaning in magnetic resonance. **D** is assumed to be determined by the dipole–dipole interaction under the point dipole approximation. This assumption is based on single crystal EPR experiments performed on a dinuclear copper complex that shows that the point dipole approximation is appropriate to characterize weakly exchange coupled interacting $S = 1/2$ spin pairs situated at least 3.4 Å apart [48]. For $S = 1/2$ pairs, interactions such as anisotropic and antisymmetric exchange are usually much weaker than the isotropic part, and are thus neglected [49, 50]. For the case of the slow EPR signal in normal water, Eq. 1 should include also the hyperfine interaction between Mo(V) ($S = 1/2$) and the solvent exchangeable proton ($I = 1/2$). As in this work, we will deal with D_2O-exchanged samples; this term will not be considered.

For two non-interacting $S = 1/2$ spins with distinct g-tensors, which in addition may have different orientations, Eq. 1 predicts for powder-like spectra two resonance lines separated by $\Delta B = h\nu\Delta g/\mu_B g_1 g_2$, in which h is the Plank constant, ν is the microwave frequency, Δg is the difference between g_1 and g_2, and $g_{i=1,2}$ are the values of the **g**-tensors for a particular direction of the spin species. Note that due to the tensorial character of **g**, ΔB depends on the orientation of the magnetic field relative to the molecular frame. When $J + D$, where D is the value of **D** for a given angle between the Mo–FeS 1 direction and the external magnetic field, is different from zero and much lower than ΔB, 1 and 2 signals are in a first-order approximation each split into doublets with a splitting equal to $J + D$. When $J + D$ is comparable with ΔB but still lower, two doublets with splitting $J + D$ are also

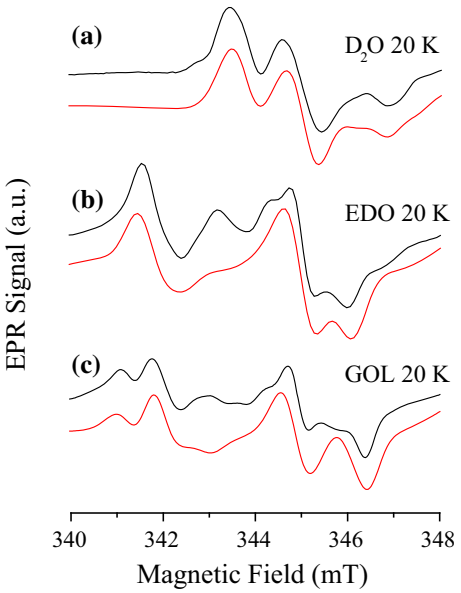

Fig. 4 EPR spectra at 20 K of the Mo(V) center together with simulations obtained using Eq. 1. *a* reduced D_2O-exchanged *Dg*AOR ($\nu = 9.64$ GHz), *b* EDO-reacted *Dg*AOR, and *c* GOL-reacted *Dg*AOR (both at $\nu = 9.49$ GHz). The small differences observed between experimental and simulation in spectra *b* and *c* are due to small amounts of slow-like EPR signal likely arising from uninhibited enzyme molecules

Table 1 EPR parameters obtained by numerical simulation using eq 1of the spectra shown in Fig. 4

Mo(V) **g**-eigenvectors	FeS 1 **g**-values	FeS 1 **g**-eigenvectors
Common parameters to all simulations		
(1,0,0)	1.939	(−0.7648, −0.6069, 0.2159)
(0,1,0)	2.023	(−0.5851, 0.5142, −0.6269)
(0,0,1)	1.950	(−0.2695, 0.6058, 0.7485)

Species	Mo(V) **g**-values (linewidths)	J ($10^{-4} \times$ cm^{-1})
Individual simulation parameters		
As-prepared (slow signal)	1.969 (0.53)	−16.6
	1.969 (0.73)	
	1.959 (0.53)	
EDO-inhibited	1.971 (0.60)	−33.3
	1.965 (0.60)	
	1.978 (0.60)	
GOL-inhibited	1.964 (0.43)	−33.3
	1.974 (0.60)	
	1.975 (0.53)	

The **D**-tensor was assumed to be axial with the unique axis lying along the Mo–FeS 1 direction ($D_z = -7.96 \times 10^{-4}$ cm^{-1}). The eigenvectors of the Mo(V) **g**-tensor (x_{Mo},y_{Mo},z_{Mo}) are referred to the molecular axes system centered in the Mo(V) ion (z_{Mo} corresponds to the Mo-OM1 direction, x_{Mo} is perpendicular to z_{Mo} and contained in the plane which includes the Mo-OM1 direction and the bisector of the Mo-S7 and Mo-S8 bonds, and y_{Mo} is perpendicular to the other two eigenvectors). Simulations were performed assuming Gaussian shaped resonance lines. Linewidths in mT are given in parenthesis

obtained but with the outer lines being less intense than the two central ones. Two lines with the same intensity separated by D are observed when $J > \Delta B$. In powder-like spectra as those shown in Fig. 2, the principal axes of the different paramagnetic species may assume all possible angles relative to the direction of the magnetic field. In such case, the EPR spectrum is spread over the entire magnetic field range determined by the different situations discussed above.

To evaluate the parameters of Eq. 1 and specially the magnitude of J, numerical simulations using Eq. 1 of the EPR spectra corresponding to reduced D_2O-exchanged *Dg*AOR and those for the alcohol-reacted enzyme were performed as explained in "Materials and methods". The results are shown in Fig. 4 together with the corresponding experimental spectra. The **D**-tensor in Eq. 1 was calculated under the point dipole approximation using the crystallographic coordinates of the Mo ion and the centroid of the FeS 1 cluster. Its diagonal components are $D_x = 3.98 \times 10^{-4}$ cm^{-1}, $D_y = 3.98 \times 10^{-4}$ cm^{-1}, $D_z = -7.96 \times 10^{-4}$ cm^{-1}, with the z axis lying along the intercenter distance. As the **g**-tensor orientations were unknown, the eigenvectors of the Mo(V) **g**-tensor for the slow signal were assigned by symmetry considerations (see Table 1), assuming that the g//axis is lying along the normal to the equatorial ligand plane. This assumption is based on the previous EPR results that showed that the slow signal is associated with a Mo(V) site with C_s or C_2 point symmetry [51] and also on results obtained from single crystal EPR spectroscopy and molecular orbital calculations on a nearly square pyramidal coordination Mo(V) complex in which the *g*//axis is lying nearly along the apical bond [52]. The principal directions of FeS 1 were also chosen from symmetry considerations, but permutations for the x, y, and z values were performed until the best agreement with the experimental spectrum was reached. Based on the X-ray data and the rhombic symmetry of the **g**-tensors, no clear assumption for the **g**-tensor orientation could be performed for EDO- and GOL-reacted *Dg*AOR. Hence, several orientations departing from the axial symmetry of the as-purified enzyme were considered keeping the principal directions of the FeS 1 **g**-tensor found for the slow signal. The **g**-tensor orientation for the Mo(V) species in the alcohol inhibited *Dg*AOR obtained with this procedure is also given in Table 1. The simulation results confirm that the FeS 1–Mo(V) exchange interaction J increases 2 times in the EDO- and GOL-reacted samples relative to that determined for the as-prepared sample (see Table 1).

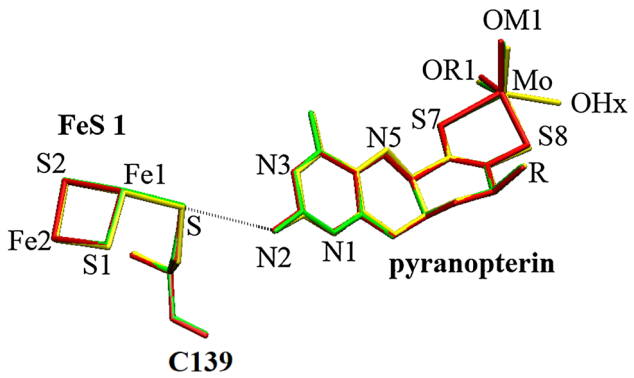

Fig. 5 Superposition of the proposed electron transfer pathway for as-prepared active *Dg*AOR (*yellow*) and reacted with different inhibitors, EDO (*red*) and GOL (*green*). The inhibitor moieties coordinated to the Mo center are omitted for simplicity

Exchange interaction and the nature of the Mo(V)–FeS 1 bridging chemical path

The magnitude of the exchange interaction is mainly determined by the distance between centers and the nature and the structural topology of the bridging chemical path [53, 54]. The dependence with distance for long bridging chemical paths was analyzed empirically by Hoffman et al. [53] on the basis of experimental data in simple inorganic systems showing weak exchange interactions ($|J| < 0.1$ cm^{-1}), who found that J decreases exponentially with distance. The topological factor is also central to determine not only the magnitude of J but also its sign, though for extended chemical bridging paths, J was always found to be antiferromagnetic ($J < 0$). The value of J can be analyzed on the basis of a qualitative model proposed by Kahn that uses non-orthogonal molecular orbitals centered at each paramagnetic species [54]. Within this frame, J is proportional to the overlap density in the bridging network, $\rho(\mathrm{i}) = \Phi 1(\mathrm{i})\Phi 2(\mathrm{i})$, where, for the system studied here, $\Phi 1$ and $\Phi 2$ are the magnetic orbitals of Mo(V) and FeS 1 centers, respectively. As *Dg*AOR presents an extended bridge between Mo and FeS 1 (see Fig. 1), the unpaired spin density should be delocalized over this large number of bridge atoms to favor the transmission of the exchange interaction.

Because of the dependence of J with distance and structural topology, we investigated in detail the different structures of *Dg*AOR obtained in the different experimental conditions analyzed in this paper. Figure 5 shows the superposition of the Mo–FeS 1 bridging pathways in the different *Dg*AOR structures. As seen in the figure, no significant differences are observed, confirming that the changes in J observed upon inhibition cannot be ascribed to structural changes associated neither with pterin and FeS 1 nor with changes in the electronic structure of FeS 1, as its EPR properties remain unchanged upon inhibition. Therefore, the changes in J detected by EPR indicate changes in the electronic structure of Mo(V), fundamentally in the spin density. These changes should be governed by structural changes experienced by the Mo center upon inhibition, as revealed by X-ray and EPR data of EDO and GOL-inhibited *Dg*AOR [31].

Unpaired spin density on the Mo center: experimental evidences and theoretical calculations

For the alcohol-inhibited *Dg*AOR samples, EPR data show that the exchange interaction increases significantly relative to reduced as-prepared *Dg*AOR, suggesting changes in the electronic structure of the Mo(V) site upon alcohol inhibition. To prove the latter, computational calculations were performed for the structures depicted in Fig. 3. First, we computed *Dg*AOR (Mo(VI)) without and with the inhibitor and with different protonation states of the Mo oxygen ligands, and compared the obtained structures with the crystallographic information available.

According to the crystallography for native *Dg*AOR (Fig. 3a), the molybdenum oxygen ligands are two oxo groups in apical (OM1) and equatorial (OR1) positions and one hydroxo group in equatorial position (OHx). In addition, the OHx ligand, which shows a larger Mo–O bond than the other two oxygen ligands, is hydrogen bonded to Glu 869. The coordination around Mo(VI) changes in EDO- and GOL-reacted *Dg*AOR due to the loss of the OHx ligand and coordination of alcohol moiety (Fig. 3c, d). In the EDO- and GOL-reacted *Dg*AOR structures, OR1 remains in oxo state but the apical OM1 ligand becomes hydroxo. A chain of water molecules close to the Mo center as well as Glu 869 are hydrogen bonded to both inhibitors helping them to maintain close to the metal atom. Also, we computed the energetic stability of apical OM1 and equatorial OR1 in hydroxo and oxo states, respectively, as reported in the crystallography, and equatorial hydroxo and apical oxo to rationalize the experimental results. We found that both inhibitors interact with Mo, but slightly different to that reported in the crystallography. Interestingly, the equatorial hydroxo and apical oxo configuration is $\sim$9 kcal/mol more favorable for EDO and $\sim$16 kcal/mol for GOL, in contrast with crystallographic results. As shown in Table 2 part a, the QM/MM computation reproduces fairly well the X-ray structure. Since we are interested in the EPR-active Mo(V) forms, we will focus our analysis on the QM/MM optimized structures shown in Table 2 part b.

As shown in Table 1, the EPR studies performed on reduced *Dg*AOR samples inhibited with glycerol and ethylene glycol showed that the value of the exchange coupling constant J increases $\sim$2 times upon alcohol

Table 2 Summary of the main metal–ligand distances (Å) from the crystallographic structures of the native enzyme and from those reacted with GOL and EDO for Mo(VI) species, together with the distances obtained from the computational calculations for Mo(VI) and Mo(V) species

(a)	Native		+EDO		+GOL	
Mo(VI)	X-ray[a]	QM/MM OM1 OR1	X-ray[b]	QM/MM OM1(oxo) OR1(hydroxo)	X-ray[c]	QM/MM OM1(oxo) OR1(hydroxo)
Mo-OM1	1.74	1.72	2.08	1.71	2.08	1.70
Mo-OR1	1.79	1.73	1.75	1.97	1.75	1.90
Mo-OHx	1.99	1.88				
Mo-S7	2.41	2.55	2.32	2.45	2.34	2.42
Mo-S8	2.49	2.66	2.39	2.50	2.41	2.47
Mo-C2			2.36	3.10	2.72	3.22
Mo-O2			2.69	2.23	2.12	2.12

(b)	Slow	+EDO		+GOL	
Mo(V) QM/MM	OM1(oxo) OR1(hydroxo) OHx	OM1(oxo) OR1(hydroxo) -O2(EDO)	OM1(hydroxo) OR1(oxo) -O2(EDO)	OM1(oxo) OR1(hydroxo) -O2(GOL)	OM1(hydroxo) OR1(oxo) -O2(GOL)
Mo-OM1	1.71	1.70	1.89	1.70	1.89
Mo-OR1	1.94	1.90	1.70	1.90	1.70
Mo-OHx	1.90				
Mo-S7	2.50	2.44	2.44	2.45	2.50
Mo-S8	2.57	2.45	2.45	2.46	2.47
Mo-C2		3.00	3.01	3.17	3.18
Mo-O2		2.15	2.17	2.11	2.10

EDO and GOL molecules were considered to be protonated for the reasons stated under the material and methods section

[a] X-ray 1.28 Å

[b] 1.79 Å

[c] 1.72 Å

inhibition and, as shown in Fig. 5, there are no significant differences in the Mo–FeS 1 bridging pathway upon alcohol inhibition. As the structural changes experienced by the Mo center upon alcohol inhibition might cause changes in the electronic structure of Mo(V), which may be translated in changes in J, we have also computed the spin density on the Mo(V)-cof upon alcohol inhibition and compared it with that of the structure associated with the slow EPR signal. The spin density is displayed in Fig. 6 for uninhibited *Dg*AOR and the enzyme including EDO or GOL as inhibitors (the pterin moiety was removed from the figure to highlight the metal). In the presence of the inhibitors, the spin density is more localized on the Mo atom and less in its O(H) ligands, changing from 86 % without the inhibitor to 97 % for EDO- and 95 % for GOL-inhibited. This change in the spin localization might increase the spin–spin interaction between the Mo atom and the FeS 1 with consequences on the EPR signal. The catalytically active OHx ligand in uninhibited *Dg*AOR possesses a spin density of $\sim$15 %, whereas the entire EDO or GOL ligands possess nearly zero spin density in the inhibited enzyme. The spin density which was present in the displaced OHx ligand is redistributed principally in the Mo(V) atom, partly in the remaining oxo and hydroxo ligands, and also on the pyranopterin moiety. As stated above and following the qualitative model proposed by Kahn, these changes in the Mo site electronic structure may be translated in an increase in the exchange coupling constant J as determined by simulation of the EPR spectra of the uninhibited and inhibited forms of *Dg*AOR.

As stated in the "Introduction", when the magnetic orbitals of the interacting spin pair and the electronic orbitals for the electron transfer reaction are the same, the maximal electron transfer rate is proportional to $|J|$ [15]. The catalytic mechanism of *Dg*AOR implies substrate binding followed by a two-electron oxidation of the reduced Mo center once the product is formed for the enzyme to start a new catalytic cycle [19]. As the two-electron transfer reaction between Mo and FeS 1 must be mediated necessarily by the pyranopterin moiety, its properties as electron transfer conduit should be modified during the catalytic cycle, i.e., suppressed during the substrate binding process and triggered during the concerted Mo reoxidation and product exit. The structure of as-purified *Dg*AOR corresponds to the ready enzyme state that starts the catalytic cycle, whereas that of alcohol-inhibited *Dg*AOR resembles the situation when the product is formed and remains within bonding distance with the Mo ion. The fact that J increases $\sim$2 times upon alcohol inhibition suggests that the electron transfer mediated by the chemical pathway Mo–FeS 1 is enhanced under these conditions, facilitating the return to the enzyme ready state. This means that the intraenzyme electron transfer process should be regulated by the catalytic labile ligand of molybdenum first coordination sphere. A ligand-based regulatory mechanism was also proposed for the electron

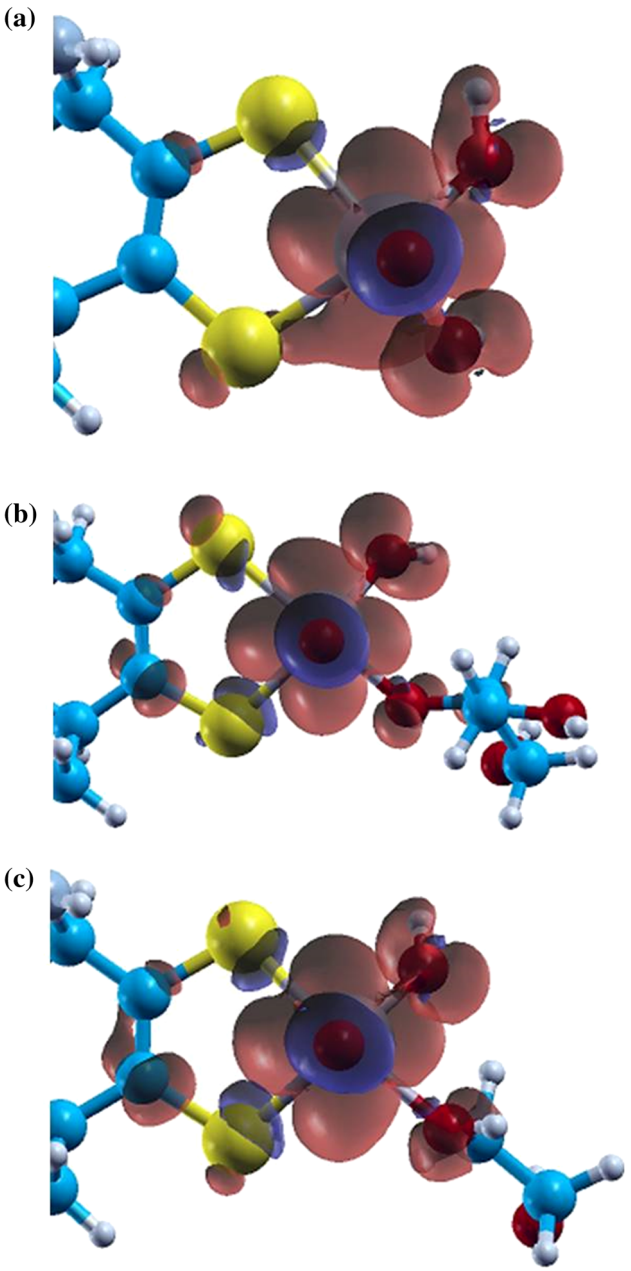

Fig. 6 Spin density maps on the EPR relevant structures of *Dg*AOR Mo site. **a** Mo(V) associated with the slow signal in the text. **b** Mo(V) + EDO inhibitor and **c** Mo(V) + GOL inhibitor. Alfa spin density is in *blue*, beta spin density in *red*. Isosurface value 0.02 e/Å^3

transfer reaction between the two quinone moieties (Q_A and Q_B) of photosystem II in bacteria, in which a bicarbonate ligand of the Fe(II) ion situated midway between Q_A and Q_B would regulate the electron flow [55].

Conclusions

The catalytic mechanism of *Dg*AOR implies the binding of substrate to the Mo(VI) center which is reduced to Mo(IV), after which Mo(IV) transfers these two reducing equivalents to an external electron acceptor through an intramolecular electron transfer reaction through the pyranopterin moiety. The different structures shown in Fig. 3 correspond to or resemble intermediate situations that occur during the redox cycling of *Dg*AOR. The oxidized state of the protein corresponds to the catalytic active form ready to bind substrate, whereas the reduced form would correspond to the Mo(V) form without bound substrate. In the alcohol-inhibited forms, the catalytic labile OHx is not present, which resembles the hypothetical situation when the reaction product is released. Considering the above-discussed experimental EPR results and the computational calculations, it is evident that the process that regulates the distribution of the unpaired spin density on the Mo(V) site is governed by the presence/absence of the equatorial OHx ligand. The catalytically active OHx ligand possesses a spin density of $\sim$15 %, and when it is not present, this spin density is redistributed principally in the Mo(V) atom, partly in the remaining oxo and hydroxo ligands and also on the pyranopterin moiety. The change in the Mo site electronic structure increases the Mo(V)–FeS 1 exchange coupling constant *J*, as clearly shown by the EPR experiments on the uninhibited and inhibited forms of *Dg*AOR. Since the relationship between electron transfer rate and isotropic exchange interaction, the present results altogether suggest that the intraenzyme electron transfer process mediated by the pyranopterin moiety is governed by a Mo ligand-based regulatory mechanism.

Supplementary material

pdb files containing atom coordinates for the 3 structures shown in Fig. 6 can be obtained from the authors upon request.

Acknowledgments We thank FONCYT, CONICET, and CAI + D-UNL in Argentina and Fundação para a Ciência e Tecnologia in Portugal for financial support. MCG and NIN thank CONICET for a fellowship grant. PJG, SDD, and CDB are members of CONICET—Argentina. Calculations were carried out on Avatar cluster at FaCAP (Facilidad de Computación de Alta Performance, Facultad de Bioquímica y Ciencias Biológicas, UNL, Santa Fe, Argentina).

References

1. Solomon EI, Sundaram UM, Machonkin TE (1996) Chem Rev 96:2563–2606
2. Boeer AB, Barra AL, Chibotaru LF, Collison D, McInnes EJL, Mole RA, Simeoni GG, Timco GA, Ungur L, Unruh T, Winpenny REP (2011) Angew Chem Int Ed 50:4007–4011
3. Kirk ML, Shultz DA, Habel-Rodriguez D, Schmidt RD, Sullivan U (2010) J Phys Chem B 114:14712–14716
4. Liu Y, Villamena FA, Rockenbauer A, Song Y, Zweier JL (2013) J Am Chem Soc 135:2350–2356

5. Hasjim PL, Ponomarenko N, Weber S, Norris JR (2010) J Phys Chem B 114:14194–14199
6. Butler WF, Calvo R, Fredkin DR, Isaacson RA, Okamura MY, Feher G (1984) Biophys J 45:947–973
7. Zatsman AI, Zhang H, Gunderson WA, Cramer WA, Hendrich MP (2006) J Am Chem Soc 128:14246–14247
8. Cheesman MR, Oganesyan VS, Watmough NJ, Butler CS, Thomson AJ (2004) J Am Chem Soc 126:4157–4166
9. Bennett B, Antholine WE, D'Souza VM, Chen G, Ustinyuk L, Holz RC (2002) J Am Chem Soc 124:13025–13034
10. More C, Camensuli P, Dole F, Guigliarelli B, Asso M, Fournel A, Bertrand P (1996) J Biol Inorg Chem 1:152–161
11. Kahn O (1993) Molecular magnetism. VCH Publishers, New York
12. Murrie M (2010) Chem Soc Rev 39:1986–1995
13. Mroziński J (2005) Coord Chem Rev 249:2534–2548
14. Benelli C, Gatteschi D (2002) Chem Rev 102:2369–2388
15. Calvo R, Isaacson RA, Paddock ML, Abresch EC, Okamura MY, Maniero AL, Brunel LC, Feher G (2001) J Phys Chem B 105:4053–4057
16. Dole F, Medina M, More C, Cammack R, Bertrand P, Guigliarelli B (1996) Biochemistry 35:16399–16406
17. González PJ, Barrera GI, Rizzi AC, Moura JJG, Passeggi MCG, Brondino CD (2009) J Inorg Biochem 103:1342–1346
18. More C, Asso M, Roger G, Guigliarelli B, Caldeira J, Moura J, Bertrand P (2005) Biochemistry 44:11628–11635
19. Brondino CD, Rivas MG, Romao MJ, Moura JJ, Moura I (2006) Acc Chem Res 39:788–796
20. Brondino CD, Romao MJ, Moura I, Moura JJ (2006) Curr Opin Chem Biol 10:109–114
21. Andrade SL, Brondino CD, Feio MJ, Moura I, Moura JJ (2000) Eur J Biochem 267:2054–2061
22. Caldeira J, Belle V, Asso M, Guigliarelli B, Moura I, Moura JJ, Bertrand P (2000) Biochemistry 39:2700–2707
23. Calvo R, Abresch EC, Bittl R, Feher G, Hofbauer W, Isaacson RA, Lubitz W, Okamura MY, Paddock ML (2000) J Am Chem Soc 122:7327–7341
24. Eaton SS, Eaton GR (1988) Coord Chem Rev 83:29–72
25. Hirsh DJ, Beck WF, Lynch JB, Que L, Brudvig GW (1992) J Am Chem Soc 114:7475–7481
26. Thapper A, Boer DR, Brondino CD, Moura JJ, Romao MJ (2007) J Biol Inorg Chem 12:353–366
27. Bertrand P, More C, Guigliarelli B, Fournel A, Bennett B, Howes B (1994) J Am Chem Soc 116:3078–3086
28. Hille R (1996) Chem Rev 96:2757–2816
29. Romao MJ, Archer M, Moura I, Moura JJ, LeGall J, Engh R, Schneider M, Hof P, Huber R (1995) Science 270:1170–1176
30. Rebelo JM, Dias JM, Huber R, Moura JJ, Romao MJ (2001) J Biol Inorg Chem 6:791–800
31. Santos-Silva T, Ferroni F, Thapper A, Marangon J, González PJ, Rizzi AC, Moura I, Moura JJG, Romão MJ, Brondino CD (2009) J Am Chem Soc 131:7990–7998
32. Andrade SL, Brondino CD, Kamenskaya EO, Levashov AV, Moura JJ (2003) Biochem Biophys Res Commun 308:73–78
33. Dobbek H (2011) Coord Chem Rev 255:1104–1116
34. Romao MJ (2009) Dalton Trans. doi:10.1039/B821108F:4053-4068
35. Moura JJ, Xavier AV, Bruschi M, Le Gall J, Hall DO, Cammack R (1976) Biochem Biophys Res Commun 72:782–789
36. Moura JJ, Xavier AV, Cammack R, Hall DO, Bruschi M, Le Gall J (1978) Biochem J 173:419–425
37. Stoll S, Schweiger A (2006) J Magn Reson 178:42–55
38. Frisch MJ, Trucks GW, Schlegel HB, Scuseria GE, Robb MA, Cheeseman JR, Scalmani G, Barone V, Mennucci B, Petersson GA, Nakatsuji H, Caricato M, Li X, Hratchian HP, Izmaylov AF, Bloino J, Zheng G, Sonnenberg JL, Hada M, Ehara M, Toyota K, Fukuda R, Hasegawa J, Ishida M, Nakajima T, Honda Y, Kitao O, Nakai H, Vreven T, Montgomery JA, Peralta JE, Ogliaro F, Bearpark M, Heyd JJ, Brothers E, Kudin KN, Staroverov VN, Kobayashi R, Normand J, Raghavachari K, Rendell A, Burant JC, Iyengar SS, Tomasi J, Cossi M, Rega N, Millam JM, Klene M, Knox JE, Cross JB, Bakken V, Adamo C, Jaramillo J, Gomperts R, Stratmann RE, Yazyev O, Austin AJ, Cammi R, Pomelli C, Ochterski JW, Martin RL, Morokuma K, Zakrzewski VG, Voth GA, Salvador P, Dannenberg JJ, Dapprich S, Daniels AD, Farkas O, Foresman JB, Ortiz JV, Cioslowski J, Fox DJ (2009) Gaussian 09, Revision A.01. Gaussian, Inc. Wallingford
39. Chai JD, Head-Gordon M (2008) Phys Chem Chem Phys 10:6615–6620
40. Ehlers AW, Böhme M, Dapprich S, Gobbi A, Höllwarth A, Jonas V, Köhler KF, Stegmann R, Veldkamp A, Frenking G (1993) Chem Phys Lett 208:111–114
41. Hay PJ, Wadt WRJ (1985) Chem Phys 82:270–283
42. Metz S, Thiel W (2009) J Am Chem Soc 131:14885–14902
43. Metz S, Wang D, Thiel W (2009) J Am Chem Soc 131:4628–4640
44. Boer DR, Thapper A, Brondino CD, Romao MJ, Moura JJ (2004) J Am Chem Soc 126:8614–8615
45. Lowe DJ, Barber MJ, Pawlik RT, Bray RC (1976) Biochem J 155:81–85
46. Gutteridge S, Tanner SJ, Bray RC (1978) Biochem J 175:887–897
47. Howes BD, Pinhal NM, Turner NA, Bray RC, Anger G, Ehrenberg A, Raynor JB, Lowe DJ (1990) Biochemistry 29:6120–6127
48. Neuman NI, Perec M, Gonzalez PJ, Passeggi MC, Rizzi AC, Brondino CD (2010) J Phys Chem A 114:13069–13075
49. Smith TD, Pilbrow JR (1974) Coord Chem Rev 13:173–278
50. Bencini A, Gatteschi D (1990) Electron paramagnetic resonance of exchange coupled systems. Springer, Berlin
51. Wilson GL, Greenwood RJ, Pilbrow JR, Spence JT, Wedd AG (1991) J Am Chem Soc 113:6803–6812
52. Cosper MM, Neese F, Astashkin AV, Carducci MD, Raitsimring AM, Enemark JH (2005) Inorg Chem 44:1290–1301
53. Hoffmann SK, Hilczer W, Goslar J (1994) Appl Magn Reson 7:289–321
54. Kahn O (1985) Angew Chem Int Ed 24:834–850
55. Fletcher S (2014) J Solid State Electrochem (In Press)